Published in final edited form as:
Nature. 2014 July 23; 511(7510): 483–487. doi:10.1038/nature13473.

Activation and repression by oncogenic Myc shape tumour-specific gene expression profiles

Susanne Walz[#1], **Francesca Lorenzin**[#1], **Jennifer Morton**[2], **Katrin E. Wiese**[1], **Björn von Eyss**[1], **Steffi Herold**[1], **Lukas Rycak**[3], **Hélène Dumay-Odelot**[4], **Saadia Karim**[2], **Marek Bartkuhn**[5], **Frederik Roels**[6], **Thorsten Wuestefeld**[7], **Matthias Fischer**[6], **Martin Teichmann**[4], **Lars Zender**[7], **Chia-Lin Wei**[8], **Owen Sansom**[2], **Elmar Wolf**[1,9,12], **Martin Eilers**[1,10,12]

[1]Theodor Boveri Institute, Biocenter, University of Würzburg, Am Hubland, 97074 Würzburg, Germany

[2]CRUK Beatson Institute, Garscube Estate, Switchback Road, Glasgow, G61 1BD, UK

[3]Institute for Molecular Biology and Tumor Research (IMT), Emil-Mannkopff-Str.2, 35033 Marburg, Germany

[4]University of Bordeaux, IECB, ARNA laboratory, Equipe Labellisée Contre le Cancer, F-33600 Pessac, France

[5]Institute for Genetics, Justus-Liebig-University, Heinrich-Buff-Ring 58, 35390 Giessen, Germany

[6]University Children's Hospital of Cologne, and Cologne Center for Molecular Medicine (CMMC), University of Cologne, Kerpener Str. 62, 50924 Cologne, Germany

[7]University Hospital Tübingen, Division of Translational Gastrointestinal Oncology, Dept. of Internal Medicine I, Otfried-Mueller-Strasse 10, 72076 Tübingen, Germany

[8]DOE Joint Genome Institute, 2800 Mitchell Drive, Walnut Creek, CA 94598, USA

[9]Rudolf Virchow Center/DFG Research Center for Experimental Biomedicine; University of Würzburg; Josef-Schneider-Str.2, 97080 Würzburg, Germany

[10]Comprehensive Cancer Center Mainfranken, University of Würzburg, Josef-Schneider-Str. 6, 97080 Würzburg, Germany

[#] These authors contributed equally to this work.

Correspondence and requests for materials should be addressed to M.E.: martin.eilers@biozentrum.uni-wuerzburg.de; E.W.: elmar.wolf@biozentrum.uni-wuerzburg.de.
[12]E.W. and M.E. should both be considered as senior authors of this study.

Author Contributions

S.W., F.L., E.W., K.E.W., B.vE. and T.W. performed the experiments, S.H., H.D-O. and M.T. characterized the Miz1 637-807 antibody, S.W., F.L., and E.W. performed ChIP-sequencing experiments, J.M. and S.K. analysed the pancreas model, F.L., F.R, M.B., M.F., S.W. and L.R. performed statistical analyses. E.W., L.Z., O.S., C.-L.W. and M.E. devised and supervised experiments and E.W. and M.E. wrote the paper.

Author Information

Microarray datasets are available at ArrayExpress under the accession number E-MTAB-1524. All ChIP- and RNA-seq datasets are available at the GEO database under the accession number GSE44672.

The authors do not declare a conflict of interest.

Europe PMC Funders Author Manuscripts

Abstract

In mammalian cells, the Myc oncoprotein binds to thousands of promoters[1–4]. During mitogenic stimulation of primary lymphocytes, Myc promotes an increase in expression of virtually all genes[1]. In contrast, Myc-driven tumour cells differ from normal cells in expression of specific sets of up- and downregulated genes that have significant prognostic value[5–7]. To understand this discrepancy, we studied the consequences of inducible expression and depletion of Myc in human cells and murine tumour models. Changes in Myc levels activate and repress specific sets of direct target genes that are characteristic of Myc-transformed tumour cells. Three factors account for this specificity: First, the magnitude of response parallels the change in occupancy by Myc at each promoter. Functionally distinct classes of target genes differ in the E-box sequence bound by Myc, arguing that different cellular responses to physiological and oncogenic Myc levels are controlled by promoter affinity. Secondly, Myc both positively and negatively affects transcription initiation independent of its effect on transcriptional elongation[8]. Third, complex formation with Miz1[9] mediates repression of multiple target genes by Myc and the ratio of Myc and Miz1 bound to each promoter correlates with the direction of response.

We expressed doxycycline-inducible Myc in U2OS cells that express low levels of endogenous Myc. Immunoblot and RQ-PCR analyses demonstrated a large increase in *MYC* mRNA leading to approximately tenfold increase in Myc protein upon addition of doxycycline (Fig. 1a and Extended Data Fig. 1a,b). Addition of doxycycline to growing cells led to marginal alterations in cell size and the percentage of BrdU-positive cells (Extended Data Fig. 1c,d). Upon prolonged exposure to doxycycline cells underwent apoptosis (Extended Data Fig.1e)[10]. Induction of Myc had no significant effect on RNA or mRNA content per cell (Extended Data Fig. 1f). ChIP-sequencing identified 20,014 peaks for endogenous Myc (Extended Data Table 1 and Extended Data Fig. 2e). Myc binding was enriched at promoters transcribed by RNA polymerases II (Pol II) and III, defining 8,401 Myc-bound Pol II promoters (Fig. 1b). Upon addition of doxycycline, the number of Myc-bound loci increased to 45,645, of which 14,903 were localized in promoters (Fig. 1b and Extended Data Fig. 3a). Consistent with previous observations, 3,656 Myc-binding sites were localized at enhancers (Extended Data Fig. 3b,c)[2].

RNA-sequencing showed that 462 genes were up- and 896 downregulated by Myc, of which 220 upregulated and 256 downregulated genes were direct target genes (Extended Data Fig. 3d). Gene set enrichment analysis (GSEA)[11] showed that Myc-regulated genes were highly similar to previously identified target genes (Extended Data Fig. 3e) and stratified human tumours according to *MYC* amplification (Extended Data Fig. 3f). Consistently, a linear support vector machine algorithm based on the set of Myc-regulated genes correctly classified 37/38 neuroblastomas as harbouring a single copy or amplified *MYCN* gene (accuracy=0.97 and Matthews correlation coefficient (mcc)=0.95).

shRNA-mediated depletion of Myc in HeLa cells, which express high levels of Myc, had no discernible effect on cell size and RNA levels per cell (Extended Data Fig. 4a,b,c). Using a cut-off of 1.5 fold change, depletion of Myc led to downregulation of 649 and upregulation of 608 genes. ChIP-sequencing identified 30,487 Myc-binding sites, 7,225 of which are located in Pol II promoters (see below at Fig. 3a,b and Extended Data Fig. 6a). Combining

both datasets showed that depletion of Myc downregulated 242 and upregulated 162 direct target genes. GSEA showed that both up- and downregulated genes were highly similar to previously identified Myc-regulated genes, correlated with signatures of Myc-regulated genes in human tumours[12] (Extended Data Fig. 4d) and allowed stratification of lung tumours according to *MYC* amplification (Extended Data Fig. 4e). A support vector machine algorithm correctly identified 37/38 neuroblastomas as harbouring an amplified or single copy *MYCN* gene (accuracy=0.97; mcc=0.95). We concluded that oncogenic Myc levels establish gene expression patterns that are characteristic of human tumour cells that express high levels of *MYC* or *MYCN*.

ChIP sequencing showed that the overall occupancy by Myc as well as the change in occupancy in response to doxycycline varied widely among promoters. The change in expression did not correlate with overall occupancy but was proportional to the change in occupancy of the respective promoter in response to doxycycline (Fig. 1c). Changes in Myc occupancy at enhancers had no consistent effect on expression of the neighbouring genes (Extended data Fig. 5a,b). GO-term analysis showed that genes encoding proteins involved in ribosome biogenesis, translation and mitochondrial function were highly occupied in proliferating cells and neither occupancy nor expression increased further when Myc expression reached supra-physiological levels (Fig. 1d,e). Target genes that mediate oncogenic effects of Myc on cell migration, angiogenesis and metastasis showed strong changes in occupancy and expression (Fig. 1d,e). The change in occupancy positively correlated with the fraction of non-consensus E-boxes (CANNTG) that are low-affinity Myc binding sites (Fig. 1f)[12]. Promoters of genes that mediate functions in cell growth were enriched for consensus E-box sequences (CACGTG) that are high affinity binding sites and their fraction was negatively correlated with the change in Myc occupancy (Fig. 1f)[12]. We concluded that differences in binding affinity enable different levels of Myc to regulate functionally distinct classes of promoters (Extended Data Fig. 5c).

Transcriptional activation by Myc involves recruitment of TFIIH and P-TEFb/Cdk9 and an increase in transcriptional elongation[8,13–16]. We therefore performed ChIP-sequencing using antibodies that recognize total Pol II, Pol II phosphorylated at serine 5 and serine 2 of the carboxyl-terminal domain (CTD), hallmarks of initiating and elongating Pol II, respectively (Fig. 2a)[17]. Changes in gene expression paralleled changes in binding of total Pol II and of Ser5-phosphorylated Pol II to the respective promoter (Fig. 2b,c). Changes in occupancy by Ser2-phosphorylated Pol II at the transcription termination site were higher than expected on activated and weaker than expected on repressed genes (Fig. 2d; p=0.00342 for the difference in slope; ANCOVA). A possible explanation is that regulation of Pol II recruitment by Myc is additive with its effect on elongation on activated genes but antagonizes it on repressed genes. Myc-induced changes in acetylation of histones H3 and H4 paralleled changes in gene expression (Fig. 2e and Extended Data Fig. 5d).

To understand how association with Miz1 affects the response to Myc, we identified 6,086 Miz-1 binding sites in HeLa cells, of which 3,270 were located in Pol II promoters (Fig. 3a and Extended Data Figs. 2a-d, 6a.b). Like Myc, binding of Miz1 paralleled occupancy of Pol II and correlated with the presence of histone H3 trimethylated at lysine 4 (H3K4me3; Fig.

3b)[1,2,15]. Genes bound by Miz1 included genes transcribed by RNA polymerase III (Extended Data Fig. 6c-f). Miz1 was not bound at enhancers (Extended Data Fig. 6g)[2].

In primary cells, Miz1 binds to a small number of sites, which contain the direct Miz1 binding sequence[18]. This sequence was detectable in only 99 of the 1,000 promoters that were most strongly bound by Miz1 and Myc, suggesting that Myc and Miz1 can bind as a complex (Extended Data Fig. 7a). Consistently, a Myc binding peak overlapped with a Miz1 peak at 2,879 core promoters ($p<2.2x10^{-308}$ based on a hypergeometric distribution; Extended Data Fig. 7b). Miz1-bound chromatin could be re-precipitated by α-Miz1, α-Myc or α-Max antibodies, demonstrating that all three proteins co-occupy target promoters (Fig. 3c and Extended Data Fig. 7c). Binding of Miz1 to promoters containing an E-box depended on Myc whereas binding to promoters with a Miz1 binding motif did not (Fig. 3d and Extended Data Fig. 7d). Induction of Myc recruited Miz1 to promoters with E-boxes (Extended Data Fig. 7e; E-box: *PPRC1*; Miz1-binding site: *VPS72*). Conversely, Myc and Max occupied Miz1-promoters in the absence of any E-box (Extended Data Fig. 7c,e,f). Myc and Miz1 also bound to promoters lacking E-Boxes and Miz1-binding sites, albeit with lower occupancy, arguing that Myc and Miz1 can bind to target sites on chromatin independently of each other or co-operatively as a complex (Extended Data Fig. 7a).

Both Myc and Miz1 are transcriptional activators that form a repressive complex upon binding to each other[19], suggesting that the Myc/Miz1 ratio at each promoter affects the direction of the response to Myc. Supporting this hypothesis, the ratio of Myc to Miz1 sequence tags at Myc-repressed promoters was around one, whereas Myc-activated genes showed a higher Myc/Miz1-ratio (Fig. 3e,f). Genes with a lower Myc/Miz1-ratio of sequence tags were regulated by Miz1, but not Myc, (Fig. 3f) and their promoters were enriched for the presence of a Miz1 binding sequence (Extended Data Fig. 8a,b; p=0.00035; Chi^2-test with Yates correction). Myc-repressed promoters had E-boxes (see Fig. 1), but lacked Miz1 binding sequences, and were enriched for binding sites of Sp1, which binds to both Myc and Miz1, arguing that protein/protein interactions affect the Myc/Miz1-ratio at each promoter (Extended Data Fig. 8c)[20,21]. shRNA-mediated depletion of Miz1 had no effect on gene activation by Myc but de-repressed by twofold or more 259/680 genes that were repressed by Myc, demonstrating that Miz1 is required for repression of a large fraction, but not all Myc target genes (Fig. 3g and Extended Data Fig. 8d). For all Myc-repressed genes, the extent of de-repression by shMiz1 correlated with their enhanced expression in cells expressing MycV394D instead of Myc; MycV394D is compromised in binding to Miz1[22] (Fig. 3g). Transcriptional activation by MycV394D was unimpaired (Extended Data Fig. 8e).

To confirm that complex formation with Miz1 is required for repression by Myc, we expressed doxycycline-inducible Myc or MycV394D in *Miz1*$^{flox/flox}$/CreER fibroblasts. In these cells, loxP sites flank exons encoding the POZ-domain and activation of CreER generates *Miz1*$^{\Delta POZ/\Delta POZ}$ cells (Fig. 4a and Extended Data Fig. 9a)[23]. Myc bound to 10,437 promoters, 4,985 of which were shared with Miz1 (of 6,876 Miz1-bound promoters; Fig. 4b). Induction of Myc repressed 2,013 genes (FC>1.5). In the presence of Myc, deletion of the POZ domain significantly enhanced expression of 1,599 genes, 541 of which were repressed by Myc ($p=5.1x10^{-125}$). For all Myc-repressed genes, the extent of de-repression

upon addition of 4-OHT closely correlated with their enhanced expression in cells expressing MycV394D instead of Myc (Fig. 4b). Deletion of the Miz1 POZ domain had virtually no effect on their expression in the absence of ectopic Myc (Extended Data Fig. 9b) and re-expression of Miz1 partially restored Myc-dependent repression in *Miz1*$^{\Delta POZ/\Delta POZ}$ cells (Extended Data Fig. 9c). MycV394D and Myc had no differential effects on expression of genes that require Miz1 for expression (Fig. 4b).

Myc bound to 36,497 sites in a doxycycline-regulatable model of Myc-driven T-lymphoma, in which repression via Miz1 is required to suppress TGFβ-induced senescence[24]. 12,125 sites were shared with Miz1 (of 25,826 Miz1 binding sites; $p<2.2x10^{-308}$; Fig. 4c; Extended Data Fig. 9d; Supplementary Information Table 1). Doxycycline-mediated repression of Myc globally reduced chromatin binding of Miz1 (Fig. 4d). The decrease in Miz1 binding was not uniform, and joint promoters fell into two classes: at one, binding of Miz1 was unaffected by Myc, whereas at the other Miz1 binding was essentially eliminated when Myc expression was suppressed (Extended Data Fig. 9e). As in human cells, the direction of the transcriptional response to Myc closely correlated with the ratio of Myc/Miz1 bound to each promoter (Fig. 4e).

Myc and Miz1 co-occupied 1,214 promoters in tumours arising in *Pdx1-Cre LSL-Kras*$^{G12D/+}$ *LSL-p53*$^{R172H/+}$-mice, in which oncogenic *KRAS* and mutant p53 are expressed in pancreatic progenitor cells (Fig. 4c and Extended Data Fig. 9f)[25]. Deletion of one allele of Myc in progenitor cells delayed tumorigenesis (Fig. 4f). Similarly, removal of one functional allele of Miz1 strongly delayed tumorigenesis, although *Miz1*$^{+/\Delta POZ}$ mice are phenotypically normal[18] (Fig. 4f). Tumorigenesis was further delayed upon removal of both functional Miz1 alleles.

We suggest that transcriptional amplification occurs when basal levels of Myc are low and association with Miz1 is absent and that changes in gene expression that occur specifically in response to oncogenic Myc levels can guide therapies targeting Myc-dependent tumours.

Methods Summary

U2OS cells were stably transfected with a doxycycline-inducible two-vector system (tet-on, Clontech) encoding a human *MYC* cDNA. Expression of Myc was induced with doxycycline (1 μg/ml) for 30 h. For depletion, HeLa cells were stably infected with a lentivirus containing an shRNA against Myc or control vector and cell pools harvested after puromycin selection. Chromatin immunoprecipitations and library generation were performed as described previously[3]. Antibodies are listed in Supplementary Information Table 2. High-throughput sequencing was performed on an Illumina GAIIx platform following the manufacturer's instructions (see details in the Methods). For Re-ChIP, chromatin was eluted with the appropriate peptide and used for a second immunoprecipitation. Genome-wide expression analysis of HeLa cells used an Agilent 44K Whole Human Genome Array. RNA-Sequencing libraries were prepared with NEBNext RNA-Seq kit and sequenced as the Chip Sequencing libraries. Statistics and bioinformatic analyses of ChIP- and RNA-sequencing experiments and microarray as well as for all experiments are described in the Extended Methods section. Oligonucleotides used are

described in Supplementary Information Table 3. The *Pdx1-Cre, LSL-Kras^{G12D}, LSL-Trp53^{R172H}* mouse model has been described previously[25]. These mice were interbred with either *c-Myc^{fl}* mice[26] or *Miz1$^{\Delta POZ}$* mice[23]. Mice on a mixed background were kept in conventional animal facilities and genotyped by Transnetyx (Cordova, TN, USA). All experiments were carried out in compliance with UK Home Office guidelines. Mice were monitored daily and sacrificed when they developed symptoms of late stage pancreatic cancer. Tumour burden was assessed by gross pathology and histology.

Methods

Cell culture and shRNA mediated gene silencing

HeLa-, HEK293T-, and U2OS cells were obtained from AATC. All cells were routinely tested for mycoplasma contamination. Cells were grown in DMEM (Sigma) supplemented with 10 % fetal calf serum (Biochrome) and penicillin/streptomycin. U2OS cells were stably transfected with a doxycycline-inducible two-vector system Myc (tet-on; Clontec Laboratories Inc.) and selected with 2.5 μg/ml hygromycin (Invitrogen). Where indicated, Myc expression was induced by addition of doxycycline (30 h; 1 μg/ml). Lentiviruses expressing an shRNA against Myc were generated using a pLKO vector (TRC-consortium) by co-transfection with the packaging plasmid psPAX.2, and the envelope plasmid pMD2.G into HEK293 cells [27]. Cells were infected with lentiviral supernatants in the presence of 4 μg/ml polybrene (Sigma) for 24 h and selected with 2.5 μg/ml puromycin. Infected cells were harvested 72-96 h after infection for analysis. The long-lived protein degradation assay was performed as described [18].

Immunofluorescence

Induced and non-induced U2OS cells were washed twice with PBS and fixed with 3.7 % paraformaldehyde. Cells were washed twice with 0.1 M glycine-PBS solution, permeabilized with 0.1 % NP-40 and then blocked with 5 % of fetal bovine serum. Anti-Myc antibody (N262) was diluted 1:200 in blocking solution and incubated 45 min at 37 °C. After washing with PBS, Alexa labelled anti-rabbit antibody incubation and PBS washing with Hoechst, the cells were mounted with Fluoromount (Sigma).

Flow cytometry analysis

Cells were labelled with 10 μM BrdU for 60 min. Afterwards, cells were fixed in 80 % ethanol overnight at -20 °C, denatured in 2 M HCl with 0.5 % Triton-X-100 for 30 min at room temperature, neutralized with 0.1 M sodium borate and stained with anti-BrdU FITC antibody. Finally, cells were resuspended in PBS with RNase A and propidium iodide, incubated for 30 min at 37 °C and analysed on a BD FACSCanto II flow cytometer. The forward light scatter (FSC) of unfixed cells was used as a relative measure of cell size.

Chromatin immunoprecipitation and parallel sequencing

Chromatin immunoprecipitations were performed as described in [28]. Cells were treated with 1 % formaldehyde for 10 min at 37 °C. After cell lysis, nuclei were re-suspended in RIPA buffer (10 mM Tris/HCl pH 7.5, 150 mM NaCl, 1 % NP40, 1 % DOC, 0.1 % SDS, 1 mM EDTA) and DNA fragmented to a size <500 bps using a Branson sonifier. To obtain specific

antibodies against Miz1, a fragment of human Miz1 (encompassing amino acids 637-803) was expressed in frame with a HIS-/GST-tandem-tag in *E. coli* (BL-21). Rabbits were immunized with the purified protein and antisera were tested for specificity by immunoblotting and immunoprecipitation. Antibodies were bound to Protein A/G-dynabeads or -sepharose (Invitrogen) and immunoprecipitated. Chromatin was eluted with 1 % SDS or alternatively with 16 μg of the appropriate peptide (Re-ChIPs, Abcam) and crosslinking was reverted overnight. For purification, the Qiagen PCR purification kit or chloroform/phenol extraction was used. ChIP-sequencing was performed as described before[3]. Purified DNA was end-repaired, A-tailed, ligated to Illumina adaptors, size selected (200 bps) and purified with Qiagen gel extraction kit. DNA fragments were amplified by 18 cycles of PCR and library size was tested with the Biorad Experion system. The amount of library DNA was quantified using a picogreen assay and subjected to Illumina GAIIx sequencing according to the manufacturer's instructions. After base calling with the Genome Analyzer Data Collection Software, high quality PF-clusters (according to the CASAVA filter) were selected for further analyses.

Q-PCRs (RT und ChIP) and global gene expression analysis

ChIP-DNA was analysed by quantitative PCR in a MX3000P (Stratagene) with Sybr green Mix (Thermo). IP or control "Cycle over threshold" (CT) values were subtracted from the input CT values and converted into percent input. To measure mRNA amount, total RNA was extracted by using the RNAeasy reagent (Qiagen). PolyA$^+$-RNA was isolated with Sera-Mag Oligo(dT) Magnetic Particles (Thermo Scientific) and quantified with NanoDrop 1000. For expression analysis total cellular RNA was isolated with the RNAeasy reagent (Qiagen) including on-column DNA digestion (microarray analysis and RNAseq) or extraction with peqGOLD TriFast (Peqlab) for reverse transcript qPCR (RT-PCR). For RT-PCR first-strand was synthesized with M-MLV Reverse Transcriptase (Invitrogen) and random hexamer primers (Roche). Primer sequences are available in Supplementary Information Table 3. For genome-wide expression analysis in HeLa cells, cRNA was synthesized, labelled and amplified with a two colour Quick-Amp Labelling Kit (Agilent p/n 5190/0444) according to the manufacturer's instructions. Labelled cRNA was hybridized on an Agilent 44K Whole Human Genome Array (G4845A 026652) and scanned with a Microarray scanner G2505C (Agilent) with 5 μm resolution at 20 bit. Raw data were generated using the Feature Extraction software v10.1.1.1 from Agilent. The resulting intensity values for the red and green channels were normalized using the lowess method within the limma package in R/BioConductor. Regulated probes were selected on the basis that the logarithmic (base 2) average intensity value (A-Value) was ≥ 5. A threshold to indicate probes as differentially expressed between two samples (M-Value) was set at 2-fold-change ($\log_2$FC = M(treatment) - M(control). Microarrays were carried out in technical duplicates for shMyc and in triplicates for empty vector.

For RNAseq in U2OS cells, PolyA$^+$-RNA was isolated from total with Sera-Mag Oligo(dT) Magnetic Particles (Thermo Scientific). Library preparation was performed by using the NEBnext® mRNA Library Prep Master Mix set for Illumina (E6100S/L) following the instruction manual. Briefly, PolyA$^+$-RNA was fragmented to generate 200 nucleotides fragments. First and second strand synthesis was performed and the resulting cDNA was

end-repaired, ligated to NEBnext Adaptor, size selected (250bps) and purified with Qiagen gel extraction kit. cDNA was then amplified with 15 cycle of PCR and the resulting library was subjected to Illumina GAIIx sequencing according to the manufacturer instructions. At several steps before and during the library preparation, quality and integrity of RNA and cDNA was assessed through an Experion™ Automated Electrophoresis System (Bio-Rad).

ChIPseq analysis

After quality control, resulting fastq files were used for alignment to a precompiled hg19 reference index with BOWTIE v0.12.7[29]. Unambiguously mapped reads were retained for subsequent generation of binding profiles, heat maps and calling of peaks. Downstream analyses were performed using R, Microsoft Excel or programs as described below. Mapped reads were used for peak calling with input or IgG sample as control and generation of .wig files with MACS v1.4.2[30] (the –keep-dup parameter was adjusted depending on the ChIP-enrichment at the highest peaks), which were visualized using the Integrated Genome Browser software[31]. To create density distributions around transcriptional start sites or ChIP peak and heat maps indicating co-occupancies Seqminer v1.3.3[32] was used. Peak annotations were achieved using the “closestBed” feature from the Bedtools suite v2.11.2[33] and the UCSC GoldenPath RefSeq database for human (hg19) or murine (mm9) genes. Intersections of ChIPseq peaks were done with the “intersectBed” tool from Bedtools and default parameters. Myc recruitment at promoters was calculated as ratio of tags in a region +/-100 bp around an annotated Myc peak summit after induction between induced and non-induced situation. Recruitment of RNA polymerase was determined as ratio of tags in a region from -100 to +300 bp relative to the TSS before and after Myc induction for all genes having an annotated Myc peak after induction. For recruitment of Pol II phosphorylated at Ser2 a region from the transcriptional end site (TES) to +2 kb downstream was analysed. To avoid 0 tags in the uninduced situation, one tag was added to all regions. Pol II promoters were defined as regions -1.5 kb/+0.5 kb relative to the transcription start site (TSS).

RNAseq analysis

Reads were alligned to the human genome with BOWTIE v0.12.8. All further analysis were performed in R/BioConductor using BAM files. For differential expression analysis EdgeRwas used [34].

Statistics and additional bioinformatic methods

Unless described differently in the figure legends, data are shown as means with standard deviation as error bars. For binned data plots, genes were sorted and grouped into equally sized bins, which were median-normalized if applicable. The median or mean value of each bin is shown and linear regression was used to illustrate trends. Fitting of the linear model to the data is given as Pearson’s correlation coefficient (r) with corresponding p-value using a Student’s t-test. To test if two linear regressions differ significantly, an analysis of covariances (ANCOVA) was applied. For the calculation of a significant overlap in a Venn diagram a hypergeometric distribution was used. Therefore the total number of base pairs covered by peaks in each ChIP-seq was calculated as well as the number of base pairs in the overlapping region. As population size all promoter regions (-1 kb to +0.5 kb relative to a TSS; total 60,336,000 bp (human) and 46,792,500 bp (mouse)) were used.

To test significant changes after Miz1 restoration in *Miz1*$^{\Delta POZ/\Delta POZ}$ fibroblasts a paired two-sided t-test was applied. Changes in Myc and Miz1 occupancies after doxycycline-induced Myc-repression in T-lymphocytes were tested to be statistically different from 0 using a one-sample t-test. To test significant changes in cell size, BrdU positive cells, RNA amount and QPCR results Student's t-tests were applied.

Functional analysis of gene groups was performed using DAVID[35]. Gene set enrichment analysis (GSEA) were performed with the C2 gene sets from the MSigDB (www.broadinstitute.org/gsea/msigdb). The number of permutations was set to 1000 and significant ($p<0.005$) gene sets related to Myc were selected. Binding motifs in Myc peaks within promoters of Myc-regulated genes were identified using the DREME algorithm within the MEME suite [36]. A region +/-100 bps around the summit of a Myc peak was analysed.

For classification of *MYCN* amplified tumours, regulated genes from Myc-depleted HeLa cells (FC>1.5) and Myc-induced U2OS cells (FC>2, p adj<0.01) were converted into probe sets and duplicates were removed. These probe sets were used to compare to 38 datasets containing 19 N-Myc amplified and 19 non-amplified samples by using a linear SVM algorithm (Support Vector Machine). The training set consisted of 96 samples. The accuracy gives the relative number of correct predictions and the Matthews correlation coefficient illustrated the fitting to the model.

Animal Studies

Power analysis was used to calculate the minimum number of mice required in each cohort to enable us to detect a significant change in survival, based on previous survival analyses in our lab. Numbers of animals were as follows: Miz$^{+/+}$ (n=15); Miz$^{\Delta POZ/+}$ (n=27); Miz$^{\Delta POZ/\Delta POZ}$ (n=16); Myc$^{+/+}$ (n=36); Myc$^{fl/+}$ (n=25). All animals were included in analysis, however animals that required to be euthanized due to non-pancreatic disease (such as lymphoma, papillomas exceeding size limits) were censored and are shown on the Kaplan-Meier curves as cross-marks. Cohorts of mice were allocated to experimental groups based on genotype. Investigators responsible for monitoring and determining the endpoints of individual mice were blinded to their genotype.

Extended Data

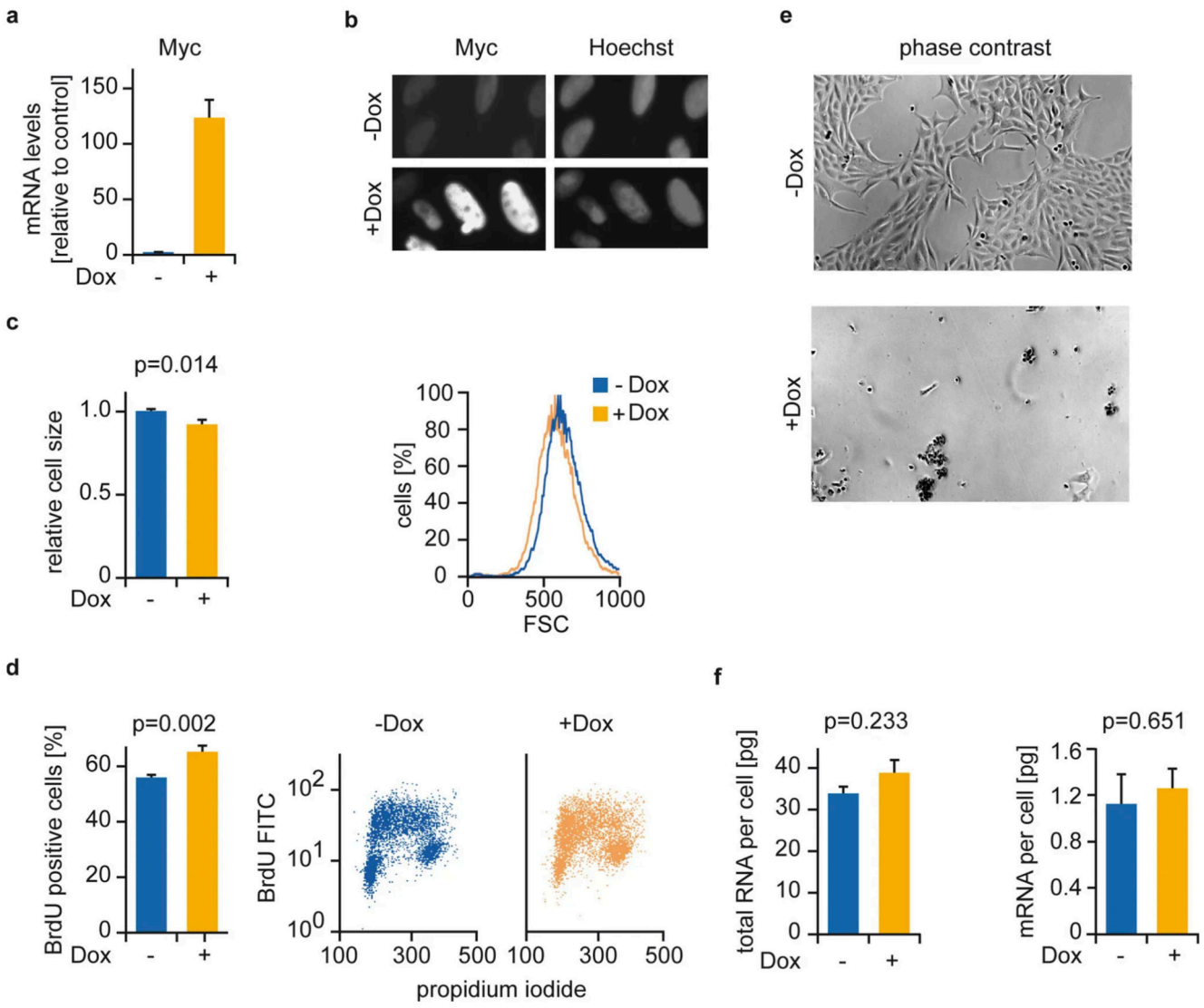

Extended Data Figure 1. Characterization of U2OS cells expressing a doxycycline-inducible allele of Myc.

a. RQ-PCR analyses demonstrating induction of *MYC* mRNA in response to doxycycline (30 h; 1 μg/ml). Error bars show SD of triplicate technical assays. Control cells were treated with ethanol.

b. Immunofluorescence using α-Myc antibody and Hoechst staining of U2OS cells before and 30 h after induction of Myc.

c. Cell size of U2OS cells before and 30 h after induction of Myc. Size was calculated from measurements of forward scatter (FSC) in arbitrary units. Errors bars show standard deviation (SD) (n=3; unless indicated otherwise, n indicates the number of independent experiments in following legends).

d. Percentage of BrdU-positive U2OS cells (left) and FACS analysis (right) documenting cell cycle distribution before and 30 h after induction of Myc with doxycycline (n=3).

e. Phase contrast pictures documenting induction of apoptosis by Myc. Pictures were taken 72 h after addition of doxycycline.

f. Amount of total RNA (left) and of mRNA (right) per cell before and after induction of Myc. Errors bars show standard error of the mean (SEM) (n=4).

Europe PMC Funders Author Manuscripts

Europe PMC Funders Author Manuscripts

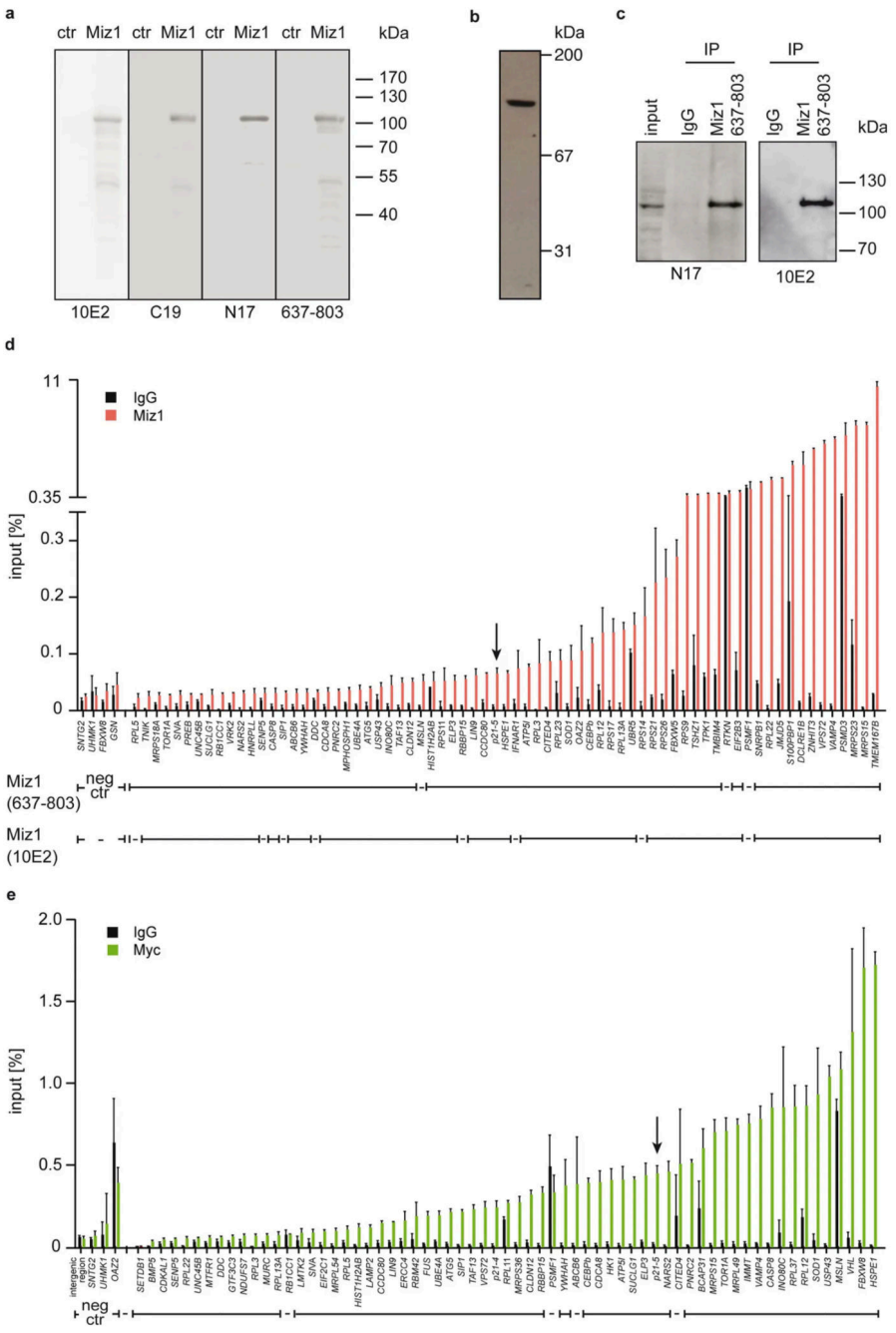

Extended Data Figure 2. Controls for antibody specificity and validation of ChIP-sequencing data.

a. HeLa cells were transfected with either control vectors or expression vectors encoding human Miz1. Cell lysates were probed with the α-Miz1 antibodies used in this study.

b. Immunoblot documenting specificity of the Miz1 (637-803) antibody used for ChIP-sequencing experiments. The blot is from nuclear extracts of IMR90 human fibroblasts.

c. Immuno-precipitations documenting that endogenous Miz1 immuno-precipitated from HeLa cells by the Miz1 (637-803) antibody is recognized by the N17 and 10E2 α-Miz1 antibodies.

d. Miz1 ChIP data for 71 randomly selected Miz1 binding sites and 4 negative controls. Shown is the percentage of input DNA precipitated by the Miz1 (637-803) antibody used for ChIP-sequencing and control IgG. Validation with a second Miz1 antibody (10E2) is shown below. "-" indicates a non-significant enrichment over IgG ($q<0.05$, heteroscedastic t-test). The arrow points to the start site of *CDKN1A* gene ("p21-5"), a known target site of Miz1.
e. Chromatin-immunoprecipitation experiments analyzing binding of Myc to randomly chosen promoters identified in the ChIP-sequencing analysis and four negative control sites. The experiment was performed using the antibody N262 in HeLa cells.

Europe PMC Funders Author Manuscripts

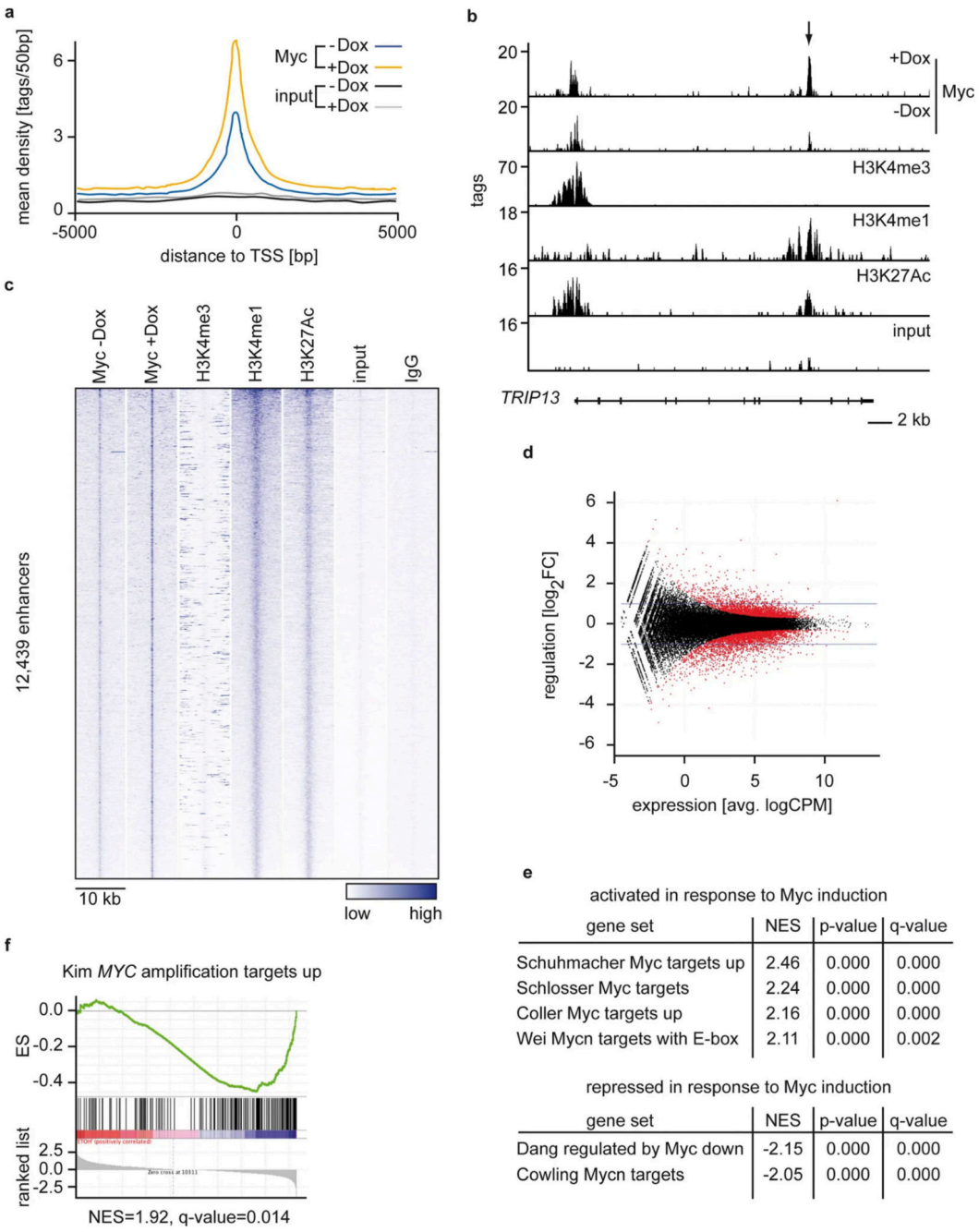

activated in response to Myc induction			
gene set	NES	p-value	q-value
Schuhmacher Myc targets up	2.46	0.000	0.000
Schlosser Myc targets	2.24	0.000	0.000
Coller Myc targets up	2.16	0.000	0.000
Wei Mycn targets with E-box	2.11	0.000	0.002

repressed in response to Myc induction			
gene set	NES	p-value	q-value
Dang regulated by Myc down	-2.15	0.000	0.000
Cowling Mycn targets	-2.05	0.000	0.000

Extended Data Figure 3. Binding of Myc to chromatin and Myc-dependent changes in gene expression in U2OS cells.

a. Distribution of Myc tags around the TSS of all human Pol II genes with and without induction of exogenous *MYC*.

b. Example of Myc-binding to a promoter and an intragenic enhancer. Enhancers are identified by the presence of H3K4me1 and H3K27Ac and the absence of H3K4me3. Exons are indicated as vertical bars, the UTR shown as a thick black line.

Europe PMC Funders Author Manuscripts

c. Heat map documenting binding of Myc to all enhancers identified in U2OS cells. Enhancer positions are centered according to Myc occupancy within a window of +/-1 kb of the centre of the enhancer region and are sorted according to the number of H3K4me1 tags.
d. The diagram shows the Myc-induced change in expression (plotted as $\log_2$FC) versus total expression levels for all genes found in the RNAseq as determined by RNA-sequencing. Red colour indicates significantly regulated genes ($q<0.01$) (n=3, biological replicates) (CPM: counts per million).
e. Myc-induced changes in gene expression are stereotypic. The panel shows a GSEA analysis of regulated genes in comparison to previously identified sets of Myc-regulated genes.
f. Enrichment plot of a GSEA analysis documenting that Myc-activated genes from U2OS cells identify lung tumours that have amplified *MYC*.

Europe PMC Funders Author Manuscripts

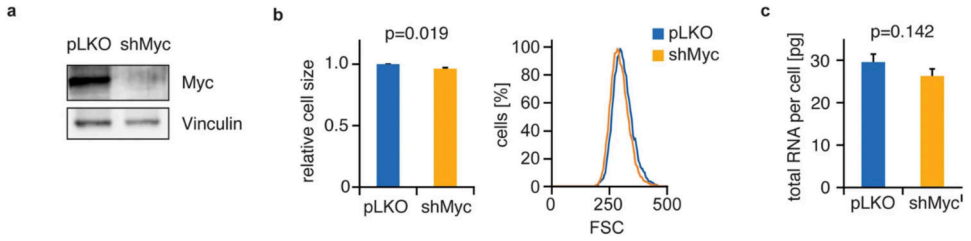

d

repressed after Myc depletion

gene set	NES	p-value	q-value
Schuhmacher Myc targets up	-2.53	0.000	0.000
Schlosser Myc targets	-2.61	0.000	0.008
Dang Myc targets up	-2.05	0.000	0.008
Benporath Myc targets with E-box	-1.77	0.000	0.090

activated after Myc depletion

gene set	NES	p-value	q-value
Cowling Mycn targets	2.18	0.000	0.001
Dang regulated by Myc down	2.12	0.000	0.002
Coller Myc targets down	1.74	0.004	0.064

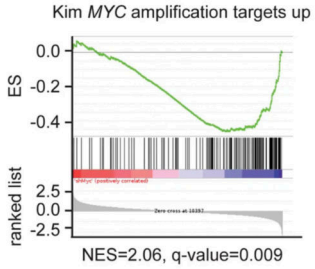

f

	clone	method	supplier
Myc	N262	ChIP, immunofluorescence	Santa Cruz
	9E10	immunoblot	Santa Cruz
Miz1	aa637-803	ChIP, immunoblot	M. Teichmann
	10E2	ChIP, immunoblot	
	N17	ChIP, immunoblot	Santa Cruz
	C19	ChIP, immunoblot	Santa Cruz
Vinculin	hVIN-1	Immunoblot	Sigma-Aldrich
RNA Pol II	N20	ChIP	Santa Cruz
	8WG16	ChIP	Covance
pSer5 Pol II	4H8	ChIP	Covance
pSer2 Pol II	ab5095	ChIP	Abcam
BrdU-FITC	B44	FACS	BD Biosciences
Max	C17	ChIP	Santa Cruz
panAc H3	06-599	ChIP	Upstate (Millipore)
panAc H4	06-866	ChIP	Upstate (Millipore)
H3K4me1	ab8895	ChIP	Abcam
H3K4me3	ab8580	ChIP	Abcam
H3K27Ac	07-360	ChIP	Upstate (Millipore)

Extended Data Figure 4. Oncogenic levels of Myc establish a tumour cell-specific pattern of gene expression in HeLa cells.

a. Immunoblots documenting Myc levels upon infection of HeLa cells with either control or lentiviruses expressing shRNA-targeting Myc. All analyses are shown for pools of stably infected and selected cells.

b. Cell size of control and Myc-depleted HeLa cells. Size was calculated from measurements of forward scatter (FSC) in arbitrary units. Errors bars show standard deviation (SD) (n=3).

c. Cellular RNA content of control and Myc-depleted HeLa cells (n=3).

d. The panels show GSEA analyses of gene sets regulated upon depletion of Myc in HeLa cells demonstrating a close overlap with previously identified sets of Myc- and N-Myc-regulated genes.

e. Stratification of human lung tumours by genes regulated in response to Myc depletion in HeLa cells. Shown is a GSEA enrichment plot with a gene set defining *MYC*-amplified lung tumours.

Europe PMC Funders Author Manuscripts

Europe PMC Funders Author Manuscripts

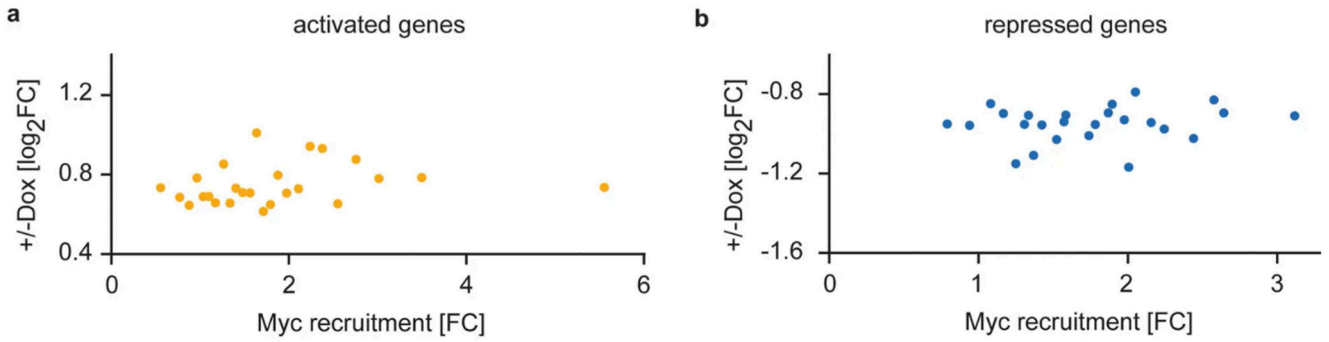

c

not regulated in response to Myc induction

GO term	q-value
mitochondrion	$1.5x10^{-2}$
cytosolic ribosome	$2.5x10^{-2}$
mRNA processing	$2.9x10^{-2}$
protein biosynthesis	$6.3x10^{-2}$

regulated in response to Myc induction

GO term	q-value
rhythmic process	$4.4x10^{-4}$
extracellular matrix	$9.8x10^{-5}$
blood vessel development	$1.4x10^{-2}$
regulation of cell death	$2.9x10^{-2}$
regulation of cell migration	$3.9x10^{-2}$
response to reactive oxygen species	$5.2x10^{-2}$

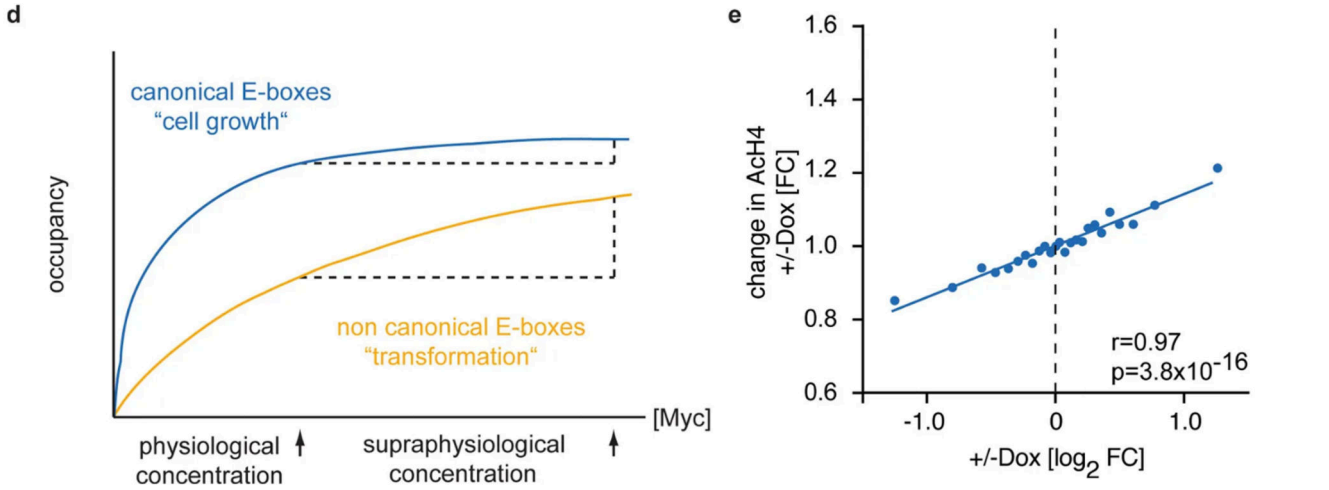

Extended Data Figure 5. Myc recruitment at enhancer regions and gene regulation.

a,b. Diagram depicting the change in gene expression versus the change in occupancy (plotted as fold recruitment) upon induction of Myc expression for 3766 enhancers that are bound by Myc and the nearest genes in U2OS cells. Panel a shows activated (n=1,457), panel b shows repressed genes (n=2,309) each diagram with 25 equally sized bins.

b. Schematic drawing summarizing the results. The annotations "cell growth" and "transformation" are meant to summarize the GO-terms of Figure 1, panel e.

d. Myc-dependent changes in histone H4 acetylation. The diagram summarizes the change in histone H4 acetylation at the promoters of all Myc-bound genes in response to induction of Myc in U2OS cells. Data are stratified by the Myc-induced change in expression (plotted as log2-sequencing). Each dot represents median values of a bin of 386 genes.

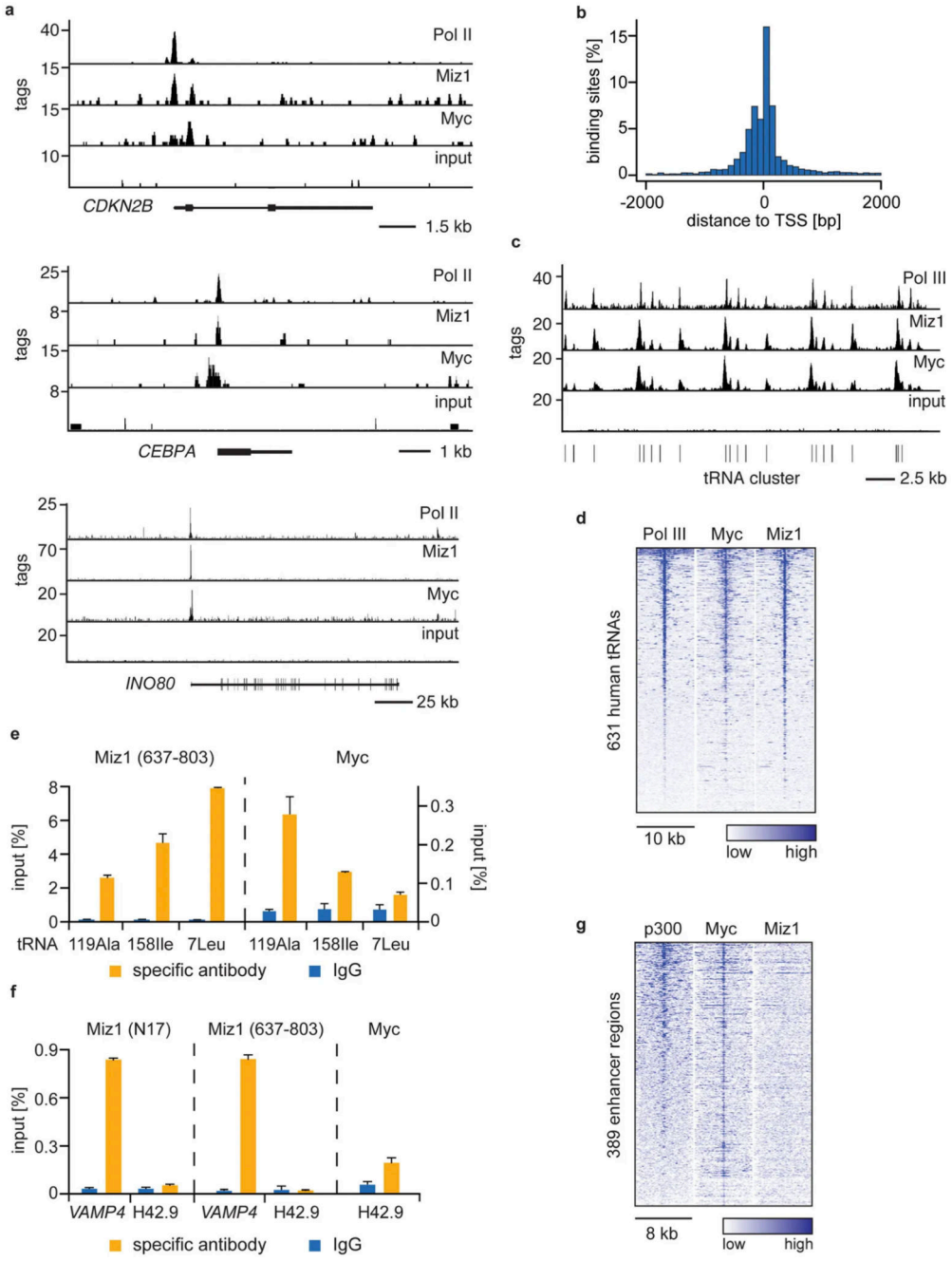

Extended Data Figure 6. Additional characterization of Miz1 binding sites on chromatin in HeLa cells.

a. Examples of ChIP-sequencing traces for two known Myc/Miz1 target genes (*CDKN2B*, *CEBPA*) and *INO80* (an E-box containing promoter).

b. Histogram showing the distribution of Miz1 binding sites relative to transcriptional start sites (TSS). The positions of Miz1 peaks are plotted relative to the next TSS of genes listed in the UCSC GoldenPath RefSeq database.

Europe PMC Funders Author Manuscripts

Europe PMC Funders Author Manuscripts

c. Genome browser picture documenting binding of Myc and Miz1 to a cluster of tRNA genes (chr1:159,675,000-159,710,000 bps). ChIP-sequencing profiles for RNA Polymerase III binding are taken from [37]. Vertical lines indicate individual tRNA genes.

d. Heat map documenting genome-wide occupancy of Myc, Miz1 and RNA Polymerase III at tRNA loci.

e. The panels show chromatin-immunoprecipitation experiments documenting binding of Myc and Miz1 to the indicated human tRNA genes. The graphs show a representative result with error bars depicting standard deviation (SD) of technical triplicates from one representative experiment (n=3).

f. The panels show chromatin-immunoprecipitation experiments analysing binding of Myc and Miz1 to ribosomal DNA cluster indicated by the oligo “H42.9”. The negative result for Miz1 was confirmed using multiple primers to scan the rRNA gene cluster, which previously have been shown to bind Myc[38]. Immuno-precipitations were performed in biological duplicates. The graphs show a representative result with error bars depicting standard deviation (SD) of technical triplicates from one experiment.

g. The heat map shows occupancy of 389 genomic regions predicted to be enhancers in HeLa cells. Enhancer regions were sorted according to p300 (ENCODE, GSM935500) occupancy and centered to the strongest Myc occupancy within a window of +/- 1 kb of the centre of the enhancer region.

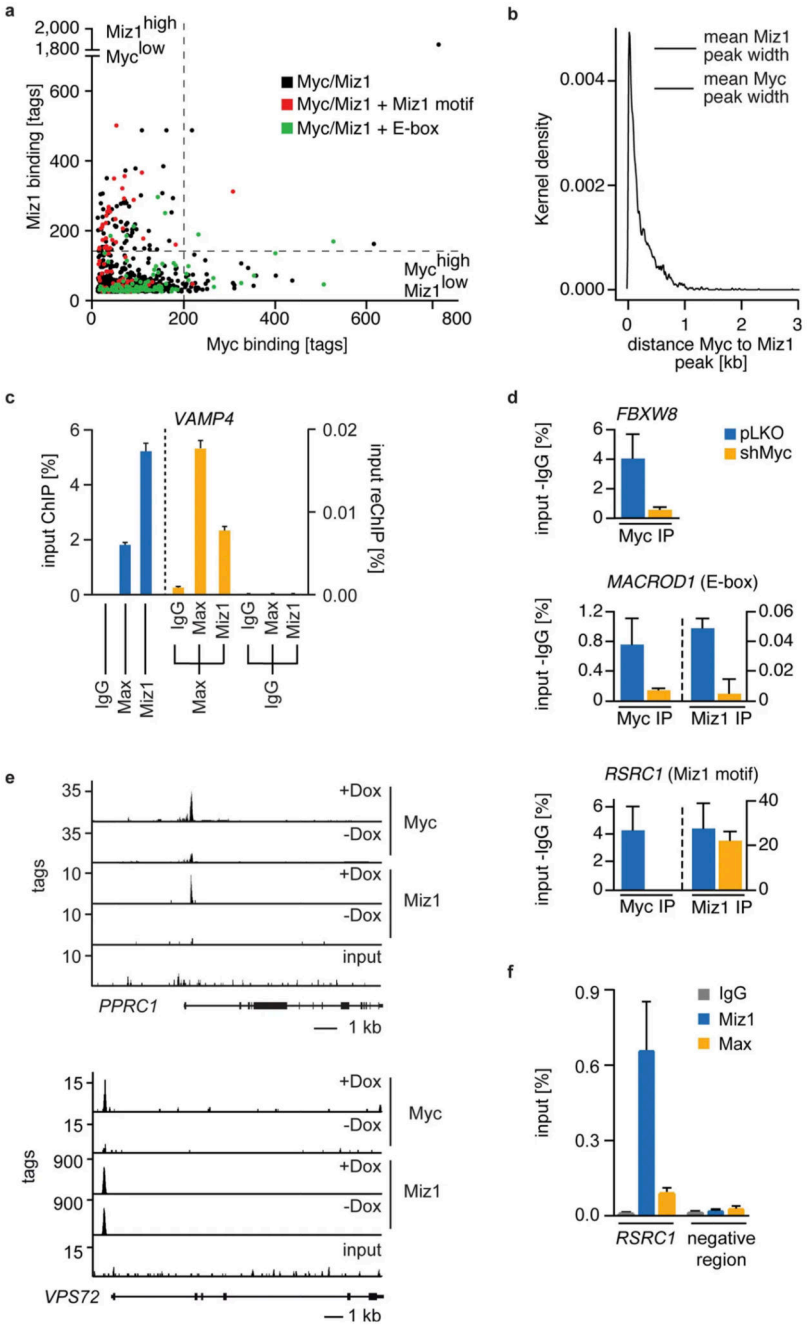

Extended Data Figure 7. Characterization of two distinct classes of Myc/Miz1 binding sites.

a. The diagram shows the number of tags for Myc and Miz1 for the 1000 most strongly Miz1-bound core promoters transcribed by Pol II in HeLa cells. Red dots indicate binding sites that have a Miz1 DNA binding motif in the Miz1 peak, green dots indicate binding sites that have an E-box (CACG/ATG) in the centre of the Myc peak (+/- 60 bps).

b. Gaussian Kernel distribution indicating close relation between Myc and Miz1 peak with a bandwidth of 10 bps. Calculated was the distance between the summit of the Myc and the

Europe PMC Funders Author Manuscripts

overlapping Miz1 peak. The mean peak width (Myc: 687 bps; Miz1:736 bps) is indicated by bars in the diagram.

c. Re-ChIP experiment of Max and Miz1 at the *VAMP4* promoter. Left: primary ChIP; right: Re-ChIP. IgG: control IgG. Error bars show SD of technical triplicates (n=2).

d. ChIP experiments documenting binding of Miz1 and Myc in control and Myc-depleted cells to the *MACROD1* (E-box) and *RSRC1* (Miz1 binding motif) promoters. *FBXW8* was used as a control for Myc depletion from chromatin on a not Miz1-bound gene. To control for experimental variation, values are normalized relative to the amount of Pol II precipitated in parallel reactions and background IgG signals were subtracted.

e. Recruitment of Miz1 by Myc to joint binding sites in U2OS cells. Representative browser pictures are from U2OS cells before and after induction of Myc.

f. ChIP experiment documenting Max and Miz1 binding to the *RSRC1* (Miz1 binding motif) promoter. The negative control region is on chromosome 11:79,556,864-79,556,942 bps.

Europe PMC Funders Author Manuscripts

Europe PMC Funders Author Manuscripts

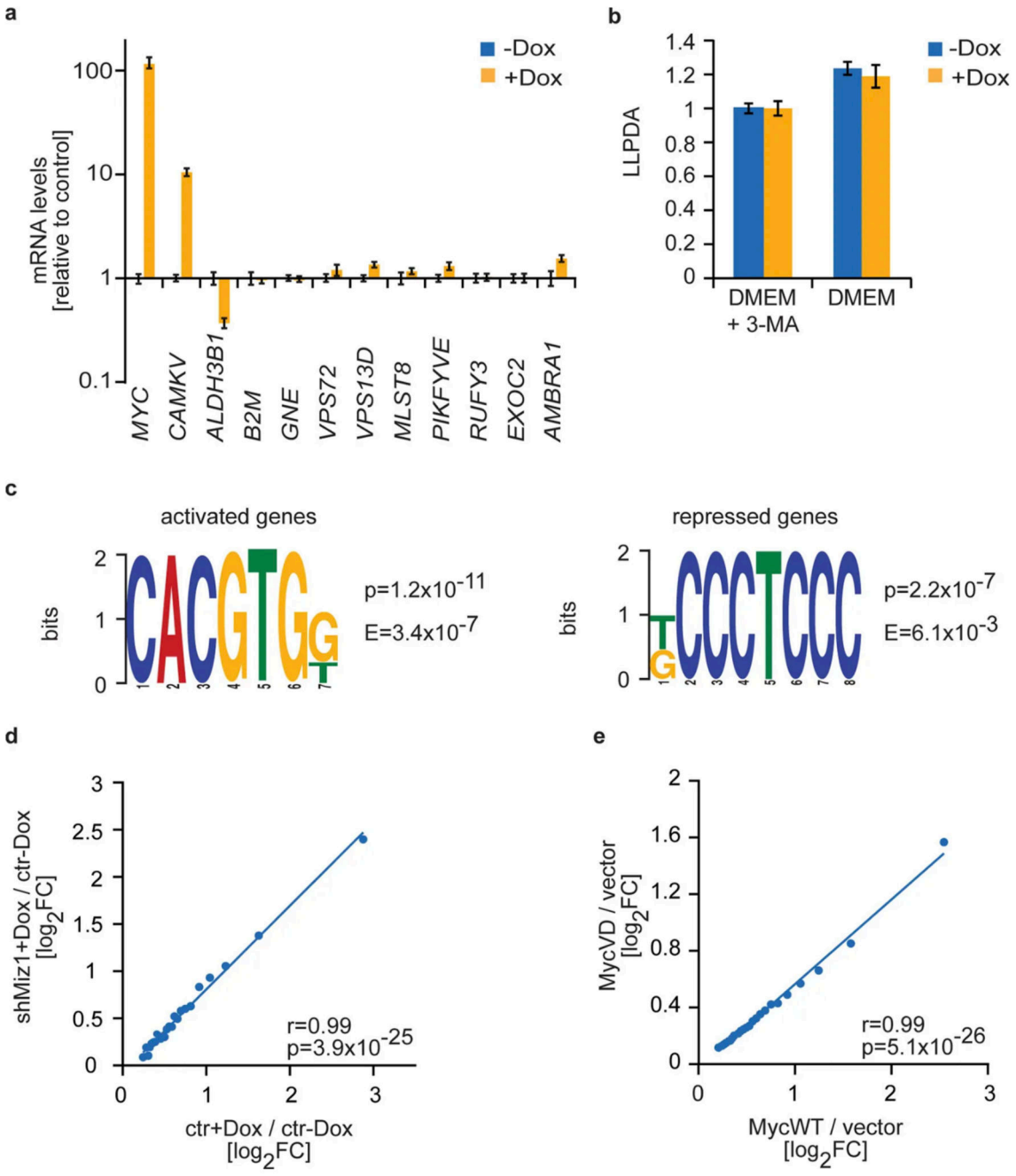

Extended Data Figure 8. Miz1 binding and transcriptional regulation by Myc.

a. RQ-PCR assays documenting no change in expression of genes that have a Miz1 consensus binding sequence in their promoter in response to addition of doxycycline to U2OS cells expressing a doxycycline-inducible allele of Myc. *CAMKV* and *ALDH3B1* are Myc regulated genes used as controls.

b. Long-lived protein degradation assay in U2OS cells in the presence and absence of doxycycline. Where indicated, 3-methyladenin (3-MA) was added to inhibit autophagy. Values are normalized to 3-MA sample. Error bars are SD of biological replicates (n=3).

c. DREME analysis showing most strong enriched motifs in 200 strongest Myc-activated and Myc-repressed genes. For the analysis the centre of the Myc peak (+/-200 bps) of peaks that are located in promoters of Myc-regulated genes was used.

d. Diagram depicting transcriptional activation of 2,787 genes upon induction of Myc in U2OS cells expressing control shRNA or shRNA targeting Miz1 ($r=0.99$; $p=3.9x10^{-25}$). Each bin summarizes expression of 112 genes.

e. Transcriptional activation of 4,637 genes upon expression MycV394D or wild-type Myc in U2OS cells ($r=0.99$; $p=5.1x10^{-26}$). 186 genes are present in each bin.

Europe PMC Funders Author Manuscripts

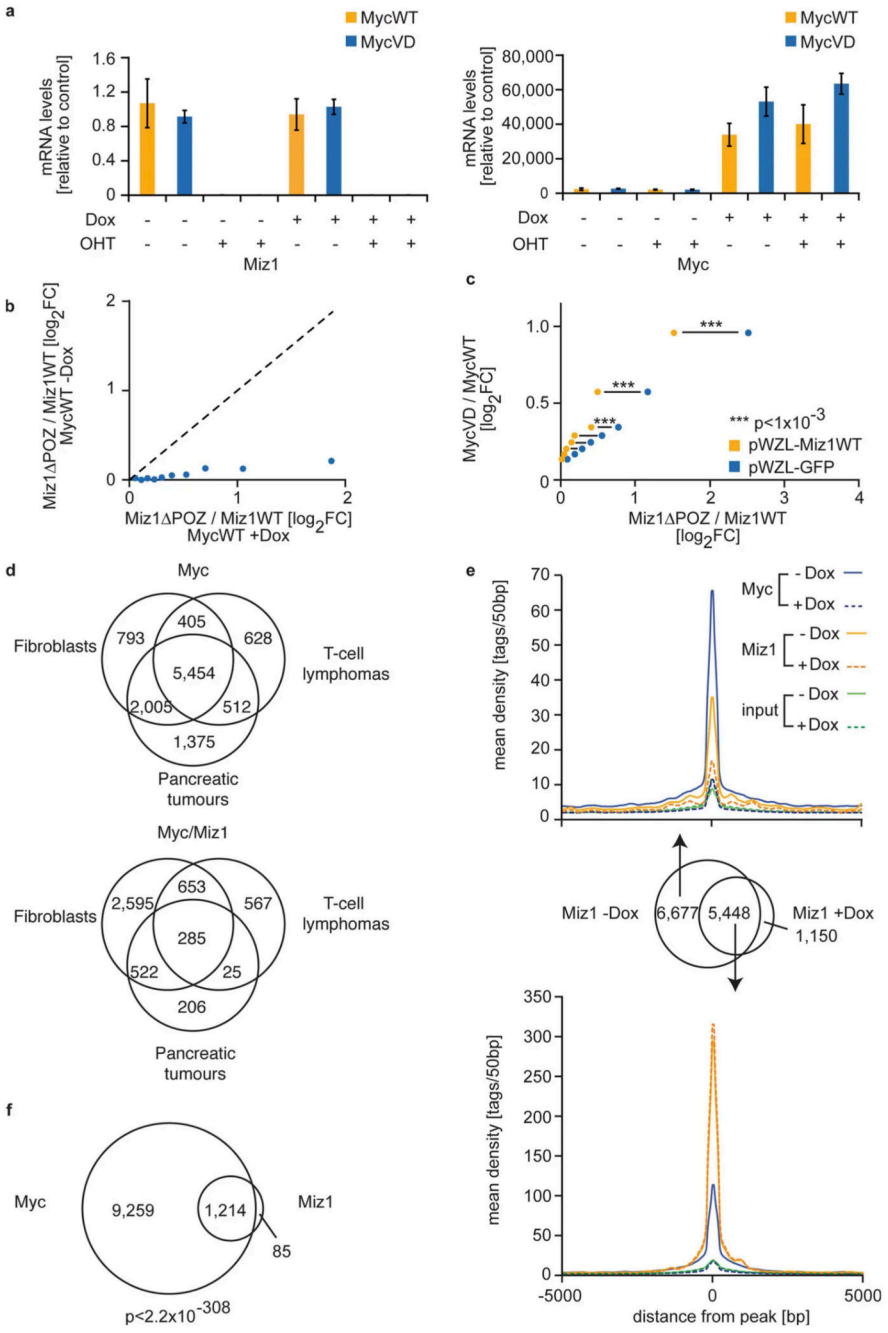

Extended Data Figure 9. Miz1 function in genetic models of Myc function.

a. RQ-PCR assays documenting removal of exons encoding the POZ domain upon addition of 4-OHT and induction of Myc or MycV394D in mouse *Miz1*$^{flox/flox}$ fibroblasts expressing a CreER recombinase.

b. Deletion of the Miz1POZ domain has virtually no effect on expression of Myc-repressed genes in the absence of induced Myc. Data are shown for bins of genes that are upregulated by deletion of the POZ domain in the presence of Myc; x-axis shows 4-OHT induced change in the presence of doxycycline, y-axis change in the absence of doxycycline.

c. Restoration of wild-type Miz1 in *Miz1*$^{\Delta POZ/\Delta POZ}$ fibroblasts re-establishes Myc-dependent repression. The data are plotted as in Fig. 4b. For each bin, a horizontal line indicates the change in expression upon restoration of Miz1. p-values indicate significance of alterations in gene expression for a given bin. p-value: two-sided paired Student's t-test.
d. Venn diagrams documenting overlap in Myc and Myc/Miz1 binding sites in murine fibroblasts, T-lymphoma cells and pancreatic tumour cells. Target gene lists are shown in Supplementary Information Table 1.
e. Myc and Miz1 binding to chromatin in T-cell lymphomas. The Venn diagram illustrates the change in Miz1 DNA binding upon doxycycline-mediated removal of Myc. Of the 12,125 sites that are bound by Myc and Miz1 in T-cell lymphomas, Miz1 remains bound at 5,448 sites in the absence of Myc.
f. Venn diagram documenting binding of Myc and Miz1 to overlapping binding sites in cells established from pancreatic tumours arising in *Kras*$^{G12D/+}$ *p53*$^{R172H/+}$-mice ($p<2.2x10^{-308}$).

Europe PMC Funders Author Manuscripts

Europe PMC Funders Author Manuscripts

Extended Data Table 1

Statistics of ChIP-sequencing reads used in the analysis.

a. ChIP-sequencing reads of U2OS used with peak calling. After performing peak calling using MACS and SICER softwares, peaks were filtered with different false discovery rate (FDR) values and used for subsequent analyses. Input control peaks were subtracted by MACS and SICER. Promoters are defined as -1.5 kb to +0.5 kb relative to the TSS. * FDR=0.1, ** FDR=1x10^{-4}, *** FDR=0.05

b. ChIP-sequencing reads of HeLa cells used with peak calling. Promoters are defined as -1.0 kb to +0.5 kb relative to the TSS.

c. ChIP-sequencing reads of T-lymphocytes cells and called binding sites using MACS software. Promoters are defined as -1.0 kb to +0.5 kb relative to the TSS.

d. ChIP-sequencing reads of cells from pancreatic tumours arising in *Kras*$^{G12D/+}$ *p53*$^{R172H/+}$- mice and called binding sites. IgG control peaks were subtracted by MACS. Promoters are defined as -1.0 kb to +0.5 kb relative to the TSS.

e. ChIP-sequencing reads in *Miz1*$^{\Delta POZ/\Delta POZ}$ fibroblasts and called binding sites using MACS software. Promoters are defined as -1.0 kb to +0.5 kb relative to the TSS.

a	HQ reads	mapped reads	binding sites	binding sites (FDR filter)	binding sites close to promoter	binding sites close to promoter (FDR 0.1)
Myc +Dox	8,481,707	7,947,678	45,696	45,645*	14,926	14,903
Myc -Dox	8,770,335	7,959,728	20,014	20,014*	8,401	8,401
Miz1 +Dox	7,187,304	5,636,366	28,186	28,186*	3,310	3,310
Miz1 -Dox	6,944,758	5,636,676	32,823	32,823*	4,195	4,195
Pol II +Dox	12,987,531	12,733,503	41,151	41,151*		
Pol 11 -Dox	12,966,907	12,736,047	37,695	37,695*		
Sers Pol II +Dox	18,083,944	17,558,426	93,397	93,397*		
Sers Pol II -Dox	17,898,479	17,563,122	73,426	73,426*		
Ser2 Pol II +Dox	8,035,906	7,526,547	71,081	71,073*		
Ser2 Pol II -Dox	7,806,811	7,544,065	62,951	62,951*		
H3K4me1 -Dox	7,264,234	7,128,027	59,256	49,074**		
H3K4me3 -Dox	6,334,300	6,138,231	23,592	23,013***		
H3K27Ac -Dox	3,921,915	3,860,049	40,188	39,613***		
panAc H3 +Dox	6,758,000	6,614,770				
panAc H3 -Dox	6,780,426	6,614,731				
panAc H4 +Dox	6,173,400	6,074,520				
panAc H4 -Dox	6,182,385	6,075,861				

a	HQ reads	mapped reads	binding sites	binding sites (FDR filter)	binding sites close to promoter	binding sites close to promoter (FDR 0.1)
input +Dox	20,666,229	20,348,902				
input -Dox	20,683,982	20,348,188				

b	HQ reads	mapped reads	binding sites	binding sites (FDR 0.1)	binding sites close to promoter	binding sites close to promoter (FDR 0.1)
Myc	24,767,282	13,664,306	30,487	30,487	7,225	7,225
Miz1	19,125,018	10,786,542	6,124	6,086	3,286	3,270
input	19,787,036	10,278,874				

c	HQ reads	mapped reads	binding sites	binding sites (FDR 0.1)	binding sites close to promoter	binding sites close to promoter (FDR 0.1)
Myc +Dox	14,453,559	13,687,224	708	20	43	2
Myc -Dox	16,598,890	13,685,221	36,948	36,947	7,752	7,752
Miz1 +Dox	14,375,816	12,935,144	19,252	12,669	5,779	4,686
Miz1 -Dox	13,612,330	12,936,309	28,627	25,826	4,867	4,572
IgG +Dox	11,461,671	10,741,676				
IgG -Dox	13,715,928	10,738,453				
input +Dox	12,435,449	11,585,216				
input -Dox	14,192,335	11,580,650				

d	HQ reads	mapped reads	binding sites	binding sites (FDR 0.1)	binding sites close to promoter	binding sites close to promoter (FDR 0.1)
Myc	13,974,887	9, 670, 044	19,700	17,375	10,976	10,473
Miz1	13,912,438	9,675,548	2,625	2,625	1,299	1,299
IgG	13,798,404	9,671,602				

e	HQ reads	mapped reads	binding sites	binding sites (FDR 0.1)	binding sites close to promoter	binding sites close to promoter (FDR 0.1)
Myc	15,767,147	10,029,924	27,910	27,910	10,437	10,437
Miz1	14,653,298	10,363,743	37,993	37,993	6,876	6,876
input	17,772,643	10,827,035				

Supplementary Material

Refer to Web version on PubMed Central for supplementary material.

Acknowledgements

This work was funded by the Deutsche Forschungsgemeinschaft via grants 222/5-3 and 222/12-1 (to M.E.), by a stipend of the graduate college 1048 ("Molecular basis of organ development in vertebrates"; to S.W.) and via the DFG Research Center for Experimental Biomedicine (to E.W.). M.T. was supported by grants from the Institut National Du Cancer (INCa) and by the Ligue National Contre le Cancer (Equipe Labellisée). Owen Sansom and Jennifer Morton are funded by a CRUK core grant and an ERC investigator grant “Coloncan”. We thank Yen Ling Lee and Thompson Poh for help with ChIP-sequencing, Florian Finkernagel (Marburg) for help with the bioinformatic analysis, Amy Au for help with mouse experiments, Bernhard Lüscher (Aachen) for critical reading of the manuscript and David Levens (NIH) for providing data prior to publication.

References

1. Nie Z, et al. c-Myc Is a Universal Amplifier of Expressed Genes in Lymphocytes and Embryonic Stem Cells. Cell. 2012; 151:68–79. [PubMed: 23021216]
2. Lin CY, et al. Transcriptional Amplification in Tumor Cells with Elevated c-Myc. Cell. 2012; 151:56–67. [PubMed: 23021215]
3. Chen X, et al. Integration of external signaling pathways with the core transcriptional network in embryonic stem cells. Cell. 2008; 133:1106–1117. [PubMed: 18555785]
4. Zeller KI, et al. Global mapping of c-Myc binding sites and target gene networks in human B cells. Proceedings of the National Academy of Sciences of the United States of America. 2006; 103:17834–17839. [PubMed: 17093053]
5. Horiuchi D, et al. MYC pathway activation in triple-negative breast cancer is synthetic lethal with CDK inhibition. J Exp Med. 2012; 209:679–696. [PubMed: 22430491]
6. Yustein JT, et al. Induction of ectopic Myc target gene JAG2 augments hypoxic growth and tumorigenesis in a human B-cell model. Proceedings of the National Academy of Sciences of the United States of America. 2010; 107:3534–3539. [PubMed: 20133585]
7. Valentijn LJ, et al. Functional MYCN signature predicts outcome of neuroblastoma irrespective of MYCN amplification. Proceedings of the National Academy of Sciences of the United States of America. 2012; 109:19190–19195. [PubMed: 23091029]
8. Rahl PB, et al. c-Myc regulates transcriptional pause release. Cell. 2010; 141:432–445. [PubMed: 20434984]
9. Wiese KE, et al. The Role of MIZ-1 in MYC-Dependent Tumorigenesis. Cold Spring Harbor perspectives in medicine. 2013; 3
10. Evan GI, et al. Induction of apoptosis in fibroblasts by c-myc protein. Cell. 1992; 69:119–128. [PubMed: 1555236]
11. Subramanian A, et al. Gene set enrichment analysis: a knowledge-based approach for interpreting genome-wide expression profiles. Proceedings of the National Academy of Sciences of the United States of America. 2005; 102:15545–15550. [PubMed: 16199517]
12. Blackwell TK, et al. Binding of Myc proteins to canonical and noncanonical DNA sequences. Mol Cell Biol. 1993; 13:5216–5224. [PubMed: 8395000]
13. Eberhardy SR, Farnham PJ. c-Myc mediates activation of the cad promoter via a post-RNA polymerase II recruitment mechanism. The Journal of biological chemistry. 2001; 276:48562–48571. [PubMed: 11673469]
14. Eberhardy SR, Farnham PJ. Myc recruits P-TEFb to mediate the final step in the transcriptional activation of the cad promoter. The Journal of biological chemistry. 2002; 277:40156–40162. [PubMed: 12177005]
15. Guccione E, et al. Myc-binding-site recognition in the human genome is determined by chromatin context. Nature cell biology. 2006; 8:764–770. [PubMed: 16767079]
16. Bouchard C, Marquardt J, Bras A, Medema RH, Eilers M. Myc-induced proliferation and transformation require Akt-mediated phosphorylation of FoxO proteins. The EMBO journal. 2004; 23:2830–2840. [PubMed: 15241468]
17. Hsin JP, Manley JL. The RNA polymerase II CTD coordinates transcription and RNA processing. Genes & development. 2012; 26:2119–2137. [PubMed: 23028141]
18. Wolf E, et al. Miz1 is required to maintain autophagic flux. Nat Commun. 2013; 4

19. Staller P, et al. Repression of p15INK4b expression by Myc through association with Miz-1. Nature cell biology. 2001; 3:392–399. [PubMed: 11283613]
20. Iraci N, et al. A SP1/MIZ1/MYCN repression complex recruits HDAC1 at the TRKA and p75NTR promoters and affects neuroblastoma malignancy by inhibiting the cell response to NGF. Cancer research. 2011; 71:404–412. [PubMed: 21123453]
21. Gartel AL, et al. Myc represses the p21(WAF1/CIP1) promoter and interacts with Sp1/Sp3. Proceedings of the National Academy of Sciences of the United States of America. 2001; 98:4510–4515. [PubMed: 11274368]
22. Herold S, et al. Negative regulation of the mammalian UV response by Myc through association with Miz-1. Mol Cell. 2002; 10:509–521. [PubMed: 12408820]
23. Kosan C, et al. Transcription factor miz-1 is required to regulate interleukin-7 receptor signaling at early commitment stages of B cell differentiation. Immunity. 2010; 33:917–928. [PubMed: 21167753]
24. van Riggelen J, et al. The interaction between Myc and Miz1 is required to antagonize TGFbeta-dependent autocrine signaling during lymphoma formation and maintenance. Genes & development. 2010; 24:1281–1294. [PubMed: 20551174]
25. Hingorani SR, et al. Trp53R172H and KrasG12D cooperate to promote chromosomal instability and widely metastatic pancreatic ductal adenocarcinoma in mice. Cancer cell. 2005; 7:469–483. [PubMed: 15894267]
26. de Alboran IM, et al. Analysis of C-MYC function in normal cells via conditional gene-targeted mutation. Immunity. 2001; 14:45–55. [PubMed: 11163229]
27. Naldini L, Blomer U, Gage FH, Trono D, Verma IM. Efficient transfer, integration, and sustained long-term expression of the transgene in adult rat brains injected with a lentiviral vector. Proceedings of the National Academy of Sciences of the United States of America. 1996; 93:11382–11388. [PubMed: 8876144]
28. Boyd KE, Farnham PJ. Myc versus USF: discrimination at the cad gene is determined by core promoter elements. Molecular and cellular biology. 1997; 17:2529–2537. [PubMed: 9111322]
29. Langmead, B. Aligning short sequencing reads with BowtieCurrent protocols in bioinformatics / editoral board. Baxevanis, Andreas D, , et al., editors. Vol. Chapter 11. 2010. 17
30. Zhang Y, et al. Model-based analysis of ChIP-Seq (MACS). Genome Biol. 2008; 9:R137. [PubMed: 18798982]
31. Nicol JW, Helt GA, Blanchard SG Jr, Raja A, Loraine AE. The Integrated Genome Browser: free software for distribution and exploration of genome-scale datasets. Bioinformatics. 2009; 25:2730–2731. [PubMed: 19654113]
32. Ye T, et al. seqMINER: an integrated ChIP-seq data interpretation platform. Nucleic Acids Res. 2011; 39:e35. [PubMed: 21177645]
33. Quinlan AR, Hall IM. BEDTools: a flexible suite of utilities for comparing genomic features. Bioinformatics. 2010; 26:841–842. [PubMed: 20110278]
34. Robinson MD, McCarthy DJ, Smyth GK. edgeR: a Bioconductor package for differential expression analysis of digital gene expression data. Bioinformatics. 2010; 26:139–140. [PubMed: 19910308]
35. Huang da W, Sherman BT, Lempicki RA. Systematic and integrative analysis of large gene lists using DAVID bioinformatics resources. Nature protocols. 2009; 4:44–57. [PubMed: 19131956]
36. Machanick P, Bailey TL. MEME-ChIP: motif analysis of large DNA datasets. Bioinformatics. 2011; 27:1696–1697. [PubMed: 21486936]
37. Barski A, et al. Pol II and its associated epigenetic marks are present at Pol III-transcribed noncoding RNA genes. Nat Struct Mol Biol. 2010; 17:629–634. [PubMed: 20418881]
38. Grandori C, et al. c-Myc binds to human ribosomal DNA and stimulates transcription of rRNA genes by RNA polymerase I. Nature cell biology. 2005; 7:311–318. [PubMed: 15723054]

Europe PMC Funders Author Manuscripts

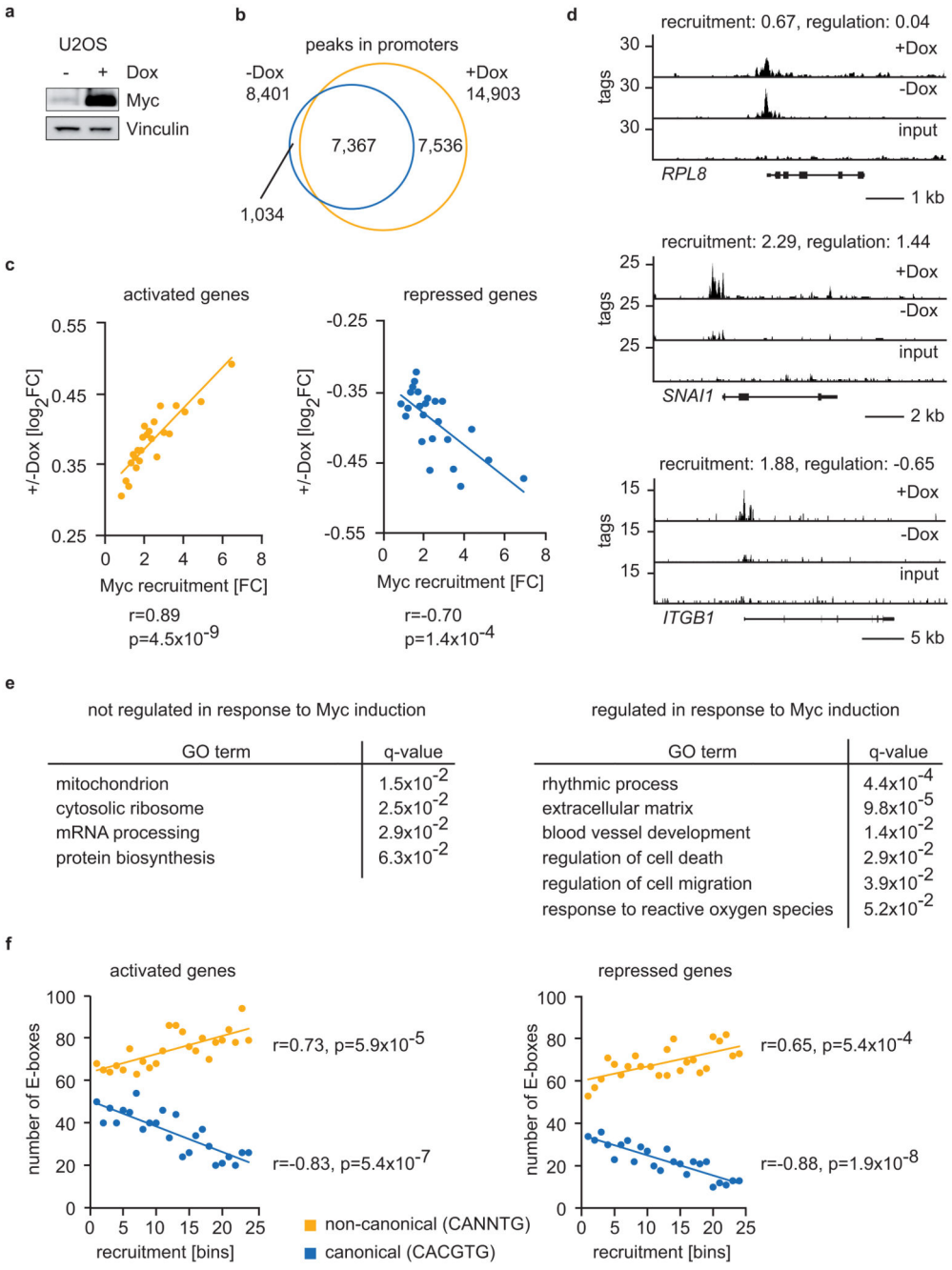

Figure 1. Oncogenic levels of Myc establish tumour cell-specific gene expression patterns.

a. Myc levels in U2OS cells before and after induction with doxycycline.

b. Number of Myc binding sites in Pol II promoters.

c. Diagram depicting change in gene expression versus change in occupancy upon induction of Myc for 9,550 promoters. Activated and repressed genes were divided into 25 bins each. p-values: two-sided Student's t-test.

d. Examples of Myc-recruitment to different promoters.

e. GO-terms of 500 Myc-bound genes that show the smallest change in gene expression and of 500 most strongly Myc-regulated genes.

f. Number of E-boxes in Myc-binding sites stratified according to change in Myc occupancy (log_2FC). p-values: two-sided Student's t-test.

Europe PMC Funders Author Manuscripts

Europe PMC Funders Author Manuscripts

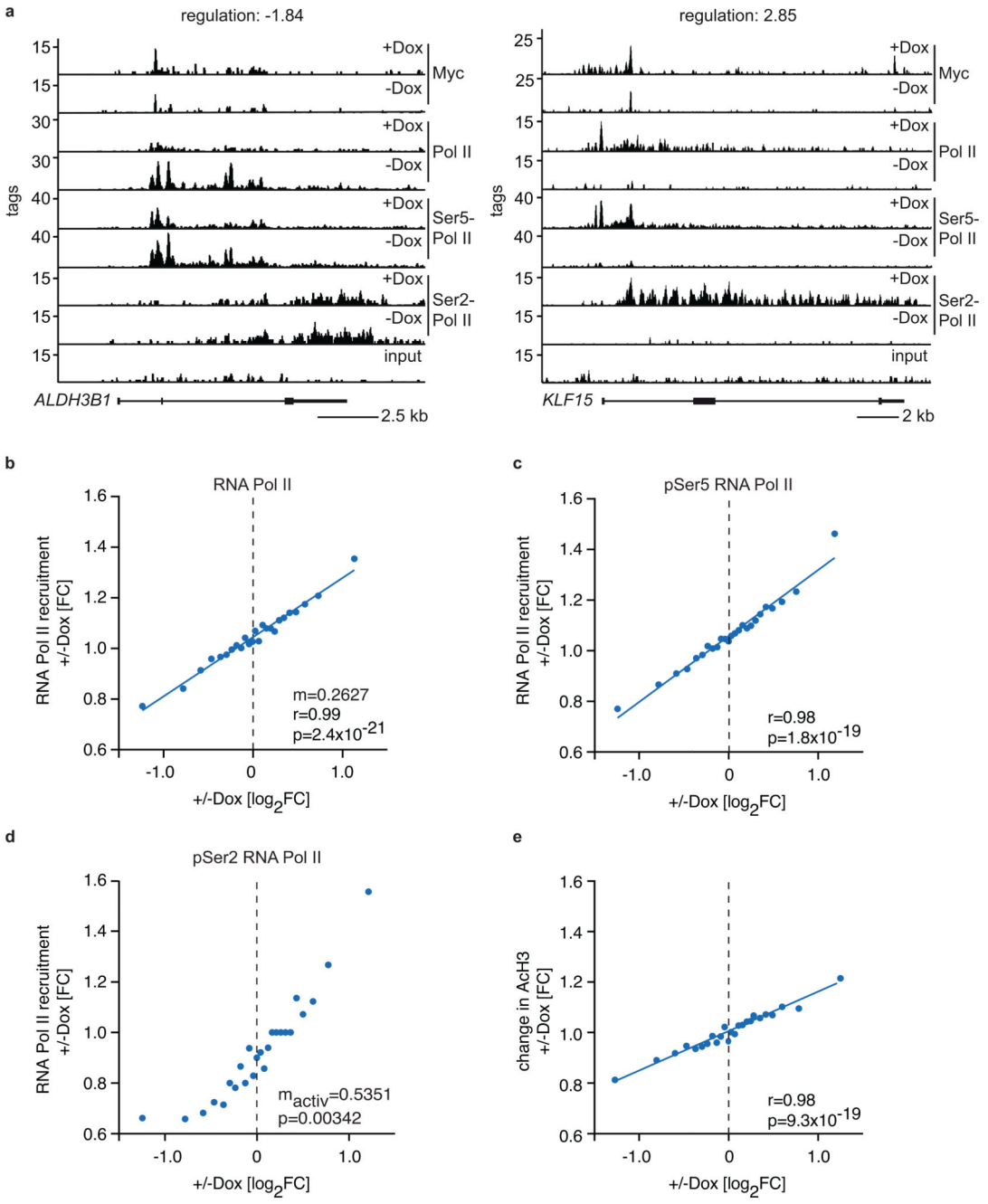

Figure 2. Myc regulates recruitment of Pol II to target promoters.

a. Examples of Pol II and Myc ChIP-sequencing traces.

b.-d. Changes in (b) total Pol II, (c) Ser5-phosphorylated Pol II and (d) Ser2-phosphorylated Pol II occupancy at Myc-bound promoters in response to induction of Myc. Data are stratified by the Myc-induced change in expression. Each bin represents median values of 380 genes. m: slope of the linear regression. r: Pearson correlation coefficient. m_{activ}; slope of regression of activated genes. p-values: two-sided Student's t-test.

e. Change in histone H3 acetylation at all Myc-bound promoters in response to Myc. Data are plotted as before.

Europe PMC Funders Author Manuscripts

Europe PMC Funders Author Manuscripts

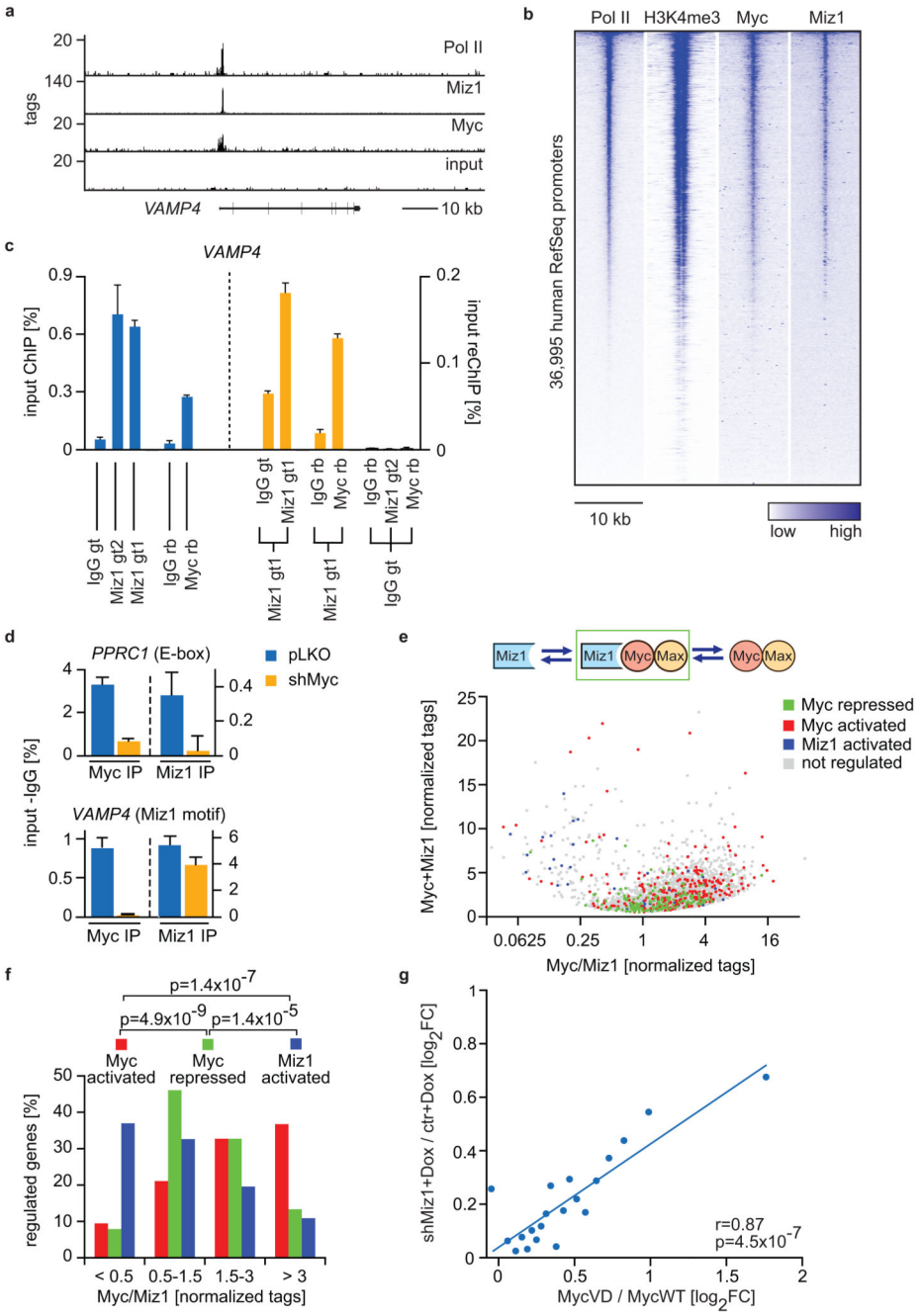

Figure 3. Characterization of joint Myc/Miz1-binding sites.

a. Example of ChIP-sequencing traces.

b. Correlation of Myc and Miz1 with Pol II binding and H3K4me3 at the TSS.

c. Re-ChIP at the *VAMP4* promoter. Left: primary ChIP; right: Re-ChIP. IgG gt:goat IgG; IgG rb: rabbit IgG. Error bars: SD of technical replicates from a representative experiment (n=3).

d. Binding of Miz1 and Myc in control and Myc-depleted cells to the *PPRC1* and *VAMP4* promoters.

e. Sum of Myc and Miz1 binding tags versus ratio of Myc/Miz1 tags.

f. Myc-activated and Myc-repressed genes stratified by the ratio of Myc/Miz1 bound to each promoter. p-values: Chi^2-test.

g. Expression of Myc-repressed genes. x-axis: difference in expression between MycV394D and Myc; y-axis: difference in Myc-dependent expression in Miz1-depleted cells relative to control cells. Each bin has 83 genes. P-value: two-sided Student's t-test.

Europe PMC Funders Author Manuscripts

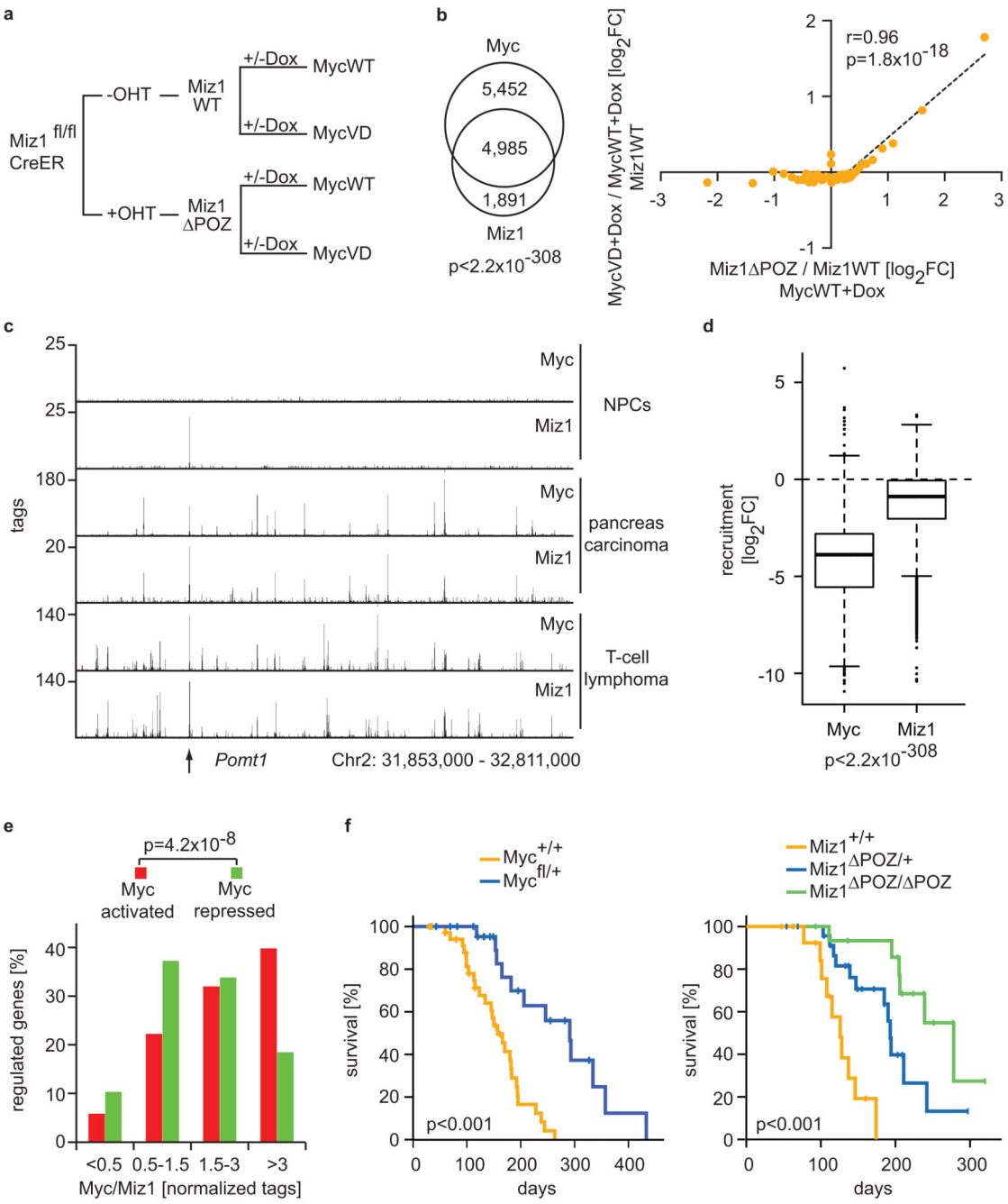

Figure 4. Role of Miz1 in Myc-dependent gene regulation and tumorigenesis.

a. Analysis of Myc-dependent changes in gene expression in Miz1$^{flox/flox}$ fibroblasts.

b. Left: Myc and Miz1 binding sites. Right: x-axis shows change in expression upon activation of CreER after induction of Myc. y-axis shows difference in expression between MycV394D and Myc. Each bin has 300 genes.

c. ChIP-sequencing traces in neuronal progenitors, T-lymphomas and pancreatic tumours. Pomt1 is a direct target of Miz1[18].

d. Changes in binding at Myc/Miz1-sites in T-lymphomas upon repression of Myc. p-values: one-sample t-test.

e. Myc-activated and -repressed genes stratified by the ratio of Myc/Miz1 bound to each promoter. p-values: Chi^2-test.

f. Kaplan-Meier survival curves of *Pdx1-creKras*$^{G12D/+}$*p53*$^{R172H/+}$-mice. Log-Rank p-values are shown.

Europe PMC Funders Author Manuscripts